

Customizing topological phases in the twisted bilayer superconductors with even-parity pairings

Conghao Lin(林丛豪), Chuanshuai Huang(黄传帅), and Xiancong Lu(卢仙聪)
Citation: Chin. Phys. B, 2023, 32 (**8**): 087401. DOI: 10.1088/1674-1056/acd3e3
Journal homepage: http://cpb.iphy.ac.cn; http://iopscience.iop.org/cpb

What follows is a list of articles you may be interested in

Superconducting properties of the C15-type Laves phase $ZrIr_2$ with an Ir-based kagome lattice

Qing-Song Yang(杨清松), Bin-Bin Ruan(阮彬彬), Meng-Hu Zhou(周孟虎), Ya-Dong Gu(谷亚东), Ming-Wei Ma(马明伟), Gen-Fu Chen(陈根富), and Zhi-An Ren(任治安)
Chin. Phys. B, 2023, 32 (**1**): 017402. DOI: 10.1088/1674-1056/aca3a2

Majorana zero modes induced by skyrmion lattice

Dong-Yang Jing(靖东洋), Huan-Yu Wang(王寰宇), Wen-Xiang Guo(郭文祥), and Wu-Ming Liu(刘伍明)
Chin. Phys. B, 2023, 32 (**1**): 017401. DOI: 10.1088/1674-1056/ac6ee7

Asymmetric Fraunhofer pattern in Josephson junctions from heterodimensional superlattice V_5S_8

Juewen Fan(范珏雯), Bingyan Jiang(江丙炎), Jiaji Zhao(赵嘉佶), Ran Bi(毕然), Jiadong Zhou(周家东), Zheng Liu(刘政), Guang Yang(杨光), Jie Shen(沈洁), Fanming Qu(屈凡明), Li Lu(吕力), Ning Kang(康宁), and Xiaosong Wu(吴孝松)
Chin. Phys. B, 2022, 31 (**5**): 057402. DOI: 10.1088/1674-1056/ac5d30

Two-dimensional square-Au_2S monolayer: A promising thermoelectric material with ultralow lattice thermal conductivity and high power factor

Wei Zhang(张伟), Xiao-Qiang Zhang(张晓强), Lei Liu(刘蕾), Zhao-Qi Wang(王朝棋), and Zhi-Guo Li(李治国)
Chin. Phys. B, 2021, 30 (**7**): 077405. DOI: 10.1088/1674-1056/abe115

Topological superconductivity in a $Bi_2Te_3/NbSe_2$ heterostructure: A review

Hao Zheng(郑浩), Jin-Feng Jia(贾金锋)
Chin. Phys. B, 2019, 28 (**6**): 067403. DOI: 10.1088/1674-1056/28/6/067403

SPECIAL TOPIC — Celebrating the 100th Anniversary of Physics Discipline of Xiamen University

Customizing topological phases in the twisted bilayer superconductors with even-parity pairings

Conghao Lin(林丛豪), Chuanshuai Huang(黄传帅), and Xiancong Lu(卢仙聪)†

Department of Physics, Xiamen University, Xiamen 361005, *China*

(Received 2 April 2023; revised manuscript received 10 May 2023; accepted manuscript online 10 May 2023)

We investigate the topological properties of twisted bilayer superconductors with different even-parity pairings in each layer. In the presence of spin–orbit coupling, the Hamiltonian is mapped into an effective odd-parity superconductor. Based on this, we deduce the topological properties by examining the relative configuration between Fermi surface and Dirac pairing node. We show that mixed Rashba and Dresselhaus spin–orbit coupling and anisotropic hopping terms, which break the C_4 symmetry of the Fermi surface, can induce first-order topological superconductors with non-zero bulk Chern number. This provides a versatile way to control the topological phases of bilayer superconductors by adjusting the twisted angle and chemical potential. We demonstrate our results using a typical twisted angle of 53.13°, at which the translation symmetry is restored and the Chern number and edge state are calculated using the Moiré momentum.

Keywords: topological superconductors, bilayer superconductors, twistronics, spin–orbit coupling

PACS: 74.78.Fk, 03.65.Vf, 71.70.Ej, 71.10.Fd **DOI:** 10.1088/1674-1056/acd3e3

1. Introduction

In the past few decades, there has been remarkable theoretical and experimental progress on the topological state of quantum matter, especially the proposal of topological superconductors.[1] Below the superconducting transition temperature, the topologically protected boundary and vortex states present a particular quasi-particle condensation, the Majorana zero modes (MZMs), which are immune to background noise by their topological nature. The MZM can allow the stable existence of the quantum bits and allow the manipulation of the quantum state from the perspective of materials, which could be used in the universal quantum computer.[2–5]

The odd-parity superconductor with a broken time-reversal symmetry and non-zero bulk Chern number has long been the most promising system for realizing a topological phase.[6] However, due to the rarity of odd-parity superconductivity pairing, whose Cooper pairs are composed of two-electron couplings belonging to different orbits with the same spin orientation,[1] this is a serious obstacle from an experimental perspective. Inspired by the research on twisted bilayer cuprates[7–12] and spin-singlet topological superconductor,[13–15] we investigate the topological properties of a twisted bilayer with different even-parity pairings, i.e., the d-wave and $s_{\pm}$-wave pairings. The d-wave pairing is common in cuprate high-temperature superconductors,[16] and the $s_{\pm}$-wave pairing is considered to play a dominant role in iron-based high-temperature superconductors.[17–19]

On the other hand, previous theoretical works show that the coupling of $s_{\pm}$-wave and d-wave pairings results in a trivial Chern number,[7,8] which can be attributed to the spin degeneracy of the normal state and the σ_v anti-symmetry of the Berry curvature.[8] In the presence of spin–orbit coupling (SOC), it has also been shown that the monolayer d + is wave superconductor is a second-order topological superconductor, holding MZMs in each corner.[20,21] Note that SOC can be incorporated into the bilayer superconductor platform in two possible ways: depositing the bilayer system on the surface of a strong topological insulator[11] or by the proximity effect with a semiconductor.[12] Moreover, SOC has also been demonstrated in cuprate Bi2212, which is considered to originate from its locally noncentrosymmetric property.[22]

Motivated by these progresses, we study the topological nature of twisted bilayer even-parity superconductors with SOC and different pairing in each layer. In contrast to previous studies on the monolayer d + is wave superconductor,[20,21] we demonstrate that breaking the C_4 symmetry of Fermi surface (FS) can induce the first-order topological superconductors with non-zero bulk Chern number. We also show that topological phases can be tuned by adjusting the twisted angle and chemical potential. This provides a versatile way to control the topological phases of the bilayer superconductors. This paper is organized as follows. In Section 2, we present the model Hamiltonian for the twisted bilayer superconductors. In Section 3, we examine the topological origin and phase transition conditions of the twisted bilayer superconductors by verifying the encirclements of Dirac pairing nodes (DPN) by FSs. We demonstrate that distorting the FS is necessary to achieve a non-zero Chern number. Finally, we provide a summary in Section 4.

†Corresponding author. E-mail: xlu@xmu.edu.cn

© 2023 Chinese Physical Society and IOP Publishing Ltd

2. Model

We consider a twisted bilayer system with different forms of superconducting pairing in each layer. Due to the addition of twist, one layer is rotated at a specific angle θ relative to the other layer. The SOC is introduced into the system through the proximity effect. Based on the tight-binding approximation, the overall model Hamiltonian consists of four terms

$$H = H_{\rm kin} + H_{\rm SOC} + H_{\rm SC} + H_{\rm t}. \tag{1}$$

Here, $H_{\rm kin}$ is the spin-independent kinetic term,

$$H_{\rm kin} = -\sum_{i,\sigma}\sum_{\hat{p}=\hat{x},\hat{y}} t_p \left(c^{\dagger}_{i\sigma l}c_{i+\hat{p},\sigma l} + {\rm h.c.}\right) - \mu\sum_{i,\sigma,l} n_{i\sigma l}, \tag{2}$$

where $c^{\dagger}_{i\sigma l}$ ($c_{i\sigma l}$) represents the creation (annihilation) of an electron at lattice site i of layer l ($l = a, b$) with spin σ, $\hat{p}$ ($\hat{p} = \hat{x}, \hat{y}$) denotes the unit lattice vector of a square lattice, t_p is the amplitude of the nearest neighbor hopping along $\hat{p}$ direction, and μ is the chemical potential. Then, $H_{\rm SOC} = H_{\rm RSOC} + H_{\rm DSOC}$ is the mixed SOC term,

$$H_{\rm RSOC} = \sum_{i,\alpha,\beta,l} {\rm i}\lambda_{\rm R}\left(c^{\dagger}_{i\alpha l}\sigma_x^{\alpha\beta}c_{i+\hat{y},\beta l} - c^{\dagger}_{i\alpha l}\sigma_y^{\alpha\beta}c_{i+\hat{x},\beta l}\right) + {\rm h.c.}, \tag{3}$$

$$H_{\rm DSOC} = \sum_{i,\alpha,\beta,l} {\rm i}\lambda_{\rm D}\left(c^{\dagger}_{i\alpha l}\sigma_x^{\alpha\beta}c_{i+\hat{x},\beta l} - c^{\dagger}_{i\alpha l}\sigma_y^{\alpha\beta}c_{i+\hat{y},\beta l}\right) + {\rm h.c.}, \tag{4}$$

with $\lambda_{\rm R(D)}$ being the amplitude of Rashba (Dresselhaus) SOC in each layer. The superconducting term $H_{\rm SC} = H^a_{\rm SC} + H^b_{\rm SC}$ includes the superconducting pairing terms in two layers ($H^a_{\rm SC}$ and $H^b_{\rm SC}$),

$$\begin{aligned} H^a_{\rm SC} = {}& \Delta_{\rm d}\sum_i \left(c^{\dagger}_{i\uparrow a}c^{\dagger}_{i+\hat{x}\downarrow a} - c^{\dagger}_{i\downarrow a}c^{\dagger}_{i+\hat{x}\uparrow a}\right. \\ & \left. - c^{\dagger}_{i\uparrow a}c^{\dagger}_{i+\hat{y}\downarrow a} + c^{\dagger}_{i\downarrow l}c^{\dagger}_{i+\hat{y}\uparrow a} + {\rm h.c.}\right), \end{aligned} \tag{5}$$

$$\begin{aligned} H^b_{\rm SC} = {}& {\rm e}^{{\rm i}\varphi}\Delta_{\rm s1}\sum_i \left(c^{\dagger}_{i\uparrow b}c_{i+\hat{x}\downarrow b} - c^{\dagger}_{i\downarrow b}c^{\dagger}_{i+\hat{x}\uparrow b}\right. \\ & \left. + c^{\dagger}_{i\uparrow b}c^{\dagger}_{i+\hat{y}\downarrow b} - c^{\dagger}_{i\downarrow b}c^{\dagger}_{i+\hat{y}\uparrow b} + {\rm h.c.}\right) \\ & + {\rm e}^{{\rm i}\varphi}\Delta_{\rm s0}\sum_i \left(c^{\dagger}_{i\uparrow b}c^{\dagger}_{i\downarrow b} - c^{\dagger}_{i\downarrow b}c^{\dagger}_{i\uparrow b} + {\rm h.c.}\right), \end{aligned} \tag{6}$$

where layer a is a d-wave superconductor with pairing amplitude $\Delta_{\rm d}$, layer b is an $s_{\pm}$-wave superconductor with pairing amplitudes $\Delta_{\rm s0}$ and $\Delta_{\rm s1}$, and the phase factor between the two superconducting layers is denoted by ${\rm e}^{{\rm i}\varphi}$. Since d-wave and $s_{\pm}$-wave superconductors belong to different symmetry classes, the phase difference φ between them will be fixed at $\varphi = \pi/2$ within the framework of Bardeen–Cooper–Schrieffer (BCS) mean-field theory,[7,8] giving rise to the time-reversal symmetry-breaking phase. Finally, $H_{\rm t}$ represents the interlayer tunneling,

$$H_{\rm t} = -\sum_{i,j,\sigma} g_{ij}c^{\dagger}_{i\sigma a}c_{j\sigma b}, \tag{7}$$

where g_{ij} is the amplitude of interlayer tunneling. In this paper, we take a simplified form for g_{ij} as in Ref. [7]

$$g_{ij} = g_0 \exp\left[-\left(r_{ij} - a_{\rm int}\right)/\rho\right], \tag{8}$$

where $r_{ij} = \sqrt{d_{ij}^2 + a_{\rm int}^2}$ is the distance between sites i and j with $a_{\rm int}$ being the distance between the two layers and d_{ij} being the in-plane separation, ρ is a decay constant, and g_0 is the intensity coefficient of interlayer tunneling. Following Ref. [7], we adopt the values $a_{\rm int} = 2.2$ and $\rho = 0.39$ in units of a_0, the lattice constant of square lattice in single layer. Note that the amplitude of interlayer tunneling will attenuate rapidly in real space.[7,9–12,23–26] Since the interlayer coupling is a minor perturbation to the superconducting order parameter, we assume that the pairing amplitudes in each layer are still uniform for a twisted system.

In the presence of a twisted angle, the translation symmetry of square lattice in a layer is normally destroyed. However, for a commensurate twisted angle $\theta = 2\arctan(n/m)$ with n and m being integers, a Moiré lattice with a lattice constant $a_{\rm M} = \sqrt{m^2+n^2}a_0$ forms. Based on the Moiré lattice, the Bloch representation can be used to calculate the Chern number and edge states numerically.[7,27] In this paper, we focus on a twisted angle $\theta = 53.13^{\circ}$ corresponding to $m = 2$ and $n = 1$; see Fig. 1.

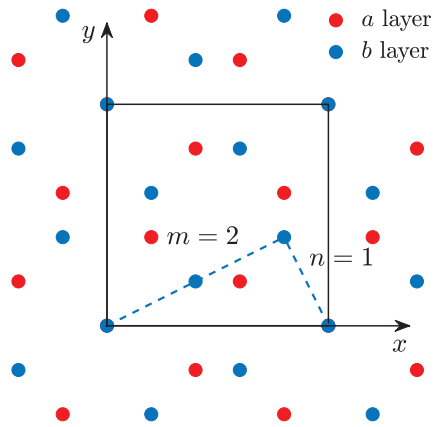


Fig. 1. Moiré lattice at twist angle $\theta = 53.13^{\circ}$. m and n are the corresponding constants.

By performing the Fourier transformation to lattices in each layer and introducing the Nambu basic vector,

$$\Psi_{\boldsymbol{k}} = \left(c^{\dagger}_{\boldsymbol{k}_a\uparrow}, c^{\dagger}_{\boldsymbol{k}_a\downarrow}, c_{-\boldsymbol{k}_a\uparrow}, c_{-\boldsymbol{k}_a\downarrow}, c^{\dagger}_{\boldsymbol{k}_b\uparrow}, c^{\dagger}_{\boldsymbol{k}_b\downarrow}, c_{-\boldsymbol{k}_b\uparrow}, c_{-\boldsymbol{k}_b\downarrow}\right)^{\rm T}, \tag{9}$$

the Hamiltonian in Eq. (1) can be rewritten into the Bogoliubov–de-Gennes (BdG) formalism

$$H = \sum_{\boldsymbol{k}} \Psi^{\dagger}_{\boldsymbol{k}} H_{{\rm BdG},\theta}(\boldsymbol{k}) \Psi_{\boldsymbol{k}}, \tag{10}$$

where $\boldsymbol{k}_a$ and $\boldsymbol{k}_b$ denote the momentums of a and b layers, and $\boldsymbol{k}$ is the momentum associated with the unrotated plane. They are connected by

$$\boldsymbol{k}_a = \boldsymbol{R}\left(\frac{\theta}{2}\right)\boldsymbol{k}, \quad \boldsymbol{k}_b = \boldsymbol{R}\left(-\frac{\theta}{2}\right)\boldsymbol{k}, \tag{11}$$

with $\boldsymbol{R}$ being the two-dimensional rotation matrix

$$\boldsymbol{R}\left(\frac{\theta}{2}\right)=\begin{pmatrix}\cos\frac{\theta}{2} & -\sin\frac{\theta}{2}\\ \sin\frac{\theta}{2} & \cos\frac{\theta}{2}\end{pmatrix}. \tag{12}$$

To gain a better understanding of the origin of the topological phase, we introduce similar transformations to map $H_{\mathrm{BdG},\theta}(\boldsymbol{k})$ into the chirality basis representation.[13,21] The details of these transformations are provided in Appendix A. After transformation, the Hamiltonian can be written as

$$H_{\mathrm{odd},\theta}(\boldsymbol{k})=\begin{pmatrix}\Sigma_\theta(\boldsymbol{k}) & \Delta_{\mathrm{odd},\theta}(\boldsymbol{k})\\ \Delta^{\dagger}_{\mathrm{odd},\theta}(\boldsymbol{k}) & -\Sigma^{\mathrm{T}}_\theta(-\boldsymbol{k})\end{pmatrix}, \tag{13}$$

in which $\Sigma_\theta(\boldsymbol{k})$ and $\Delta_{\mathrm{odd},\theta}(\boldsymbol{k})$ are 4×4 matrices given by Eqs. (A14) and (A15) in Appendix A, respectively. Since

$$\begin{aligned}-\Delta_{\mathrm{odd},\theta}(-\boldsymbol{k}) &= \begin{pmatrix}-\tilde{\Delta}_a(-\boldsymbol{k}_a) & 0\\ 0 & -\tilde{\Delta}_b(-\boldsymbol{k}_b)\end{pmatrix}\\ &= \Delta_{\mathrm{odd},\theta}(\boldsymbol{k}),\end{aligned} \tag{14}$$

the Hamiltonian $H_{\mathrm{odd},\theta}(\boldsymbol{k})$ is an effective odd parity superconductor.[21,28] The topological property of $H_{\mathrm{BdG},\theta}(\boldsymbol{k})$ can be deduced by analyzing $H_{\mathrm{odd},\theta}(\boldsymbol{k})$ for the chirality basis transformation does not change the topological invariant.[13]

3. Topological properties

With the help of SOC, the bilayer system can be regarded as an effective odd-parity superconductor, whose band topology is determined by the relative configuration of the FSs and the DPNs.[28,29] If a FS encloses a DPN, FS cannot shrink to disappear continuously because it surrounds a zero-dimensional non-trivial point in two-dimensional space.[29] The Dirac pairing nodes (not the time-reversal invariant point) are zeroes of $\Delta_{\mathrm{odd},\theta}(\boldsymbol{k})$, which can be obtained by solving $\Delta_a(\boldsymbol{k}_a)=0$ and $\Delta_b(\boldsymbol{k}_b)=0$. The four DPNs $\boldsymbol{Q}_i$ $(i=1,2,3,4)$ are located at the intersections of nodal lines of d-wave and $s_\pm$-wave pairings (see Fig. 2), given by

$$\boldsymbol{Q}_i=\boldsymbol{R}\left(\frac{\theta+(i-1)\pi}{2}\right)\boldsymbol{K}, \tag{15}$$

where $\boldsymbol{R}(\phi)$ is the two-dimensional rotation matrix and $\boldsymbol{K}=(K,K)$ are determined by the equation

$$2\cos\left[\cos(\theta)K\right]\cos\left[\sin(\theta)K\right]=-\frac{\Delta_{\mathrm{s0}}}{2\Delta_{\mathrm{s1}}}. \tag{16}$$

Since the positions of DPNs depend on the ratio $\Delta_{\mathrm{s0}}/\Delta_{\mathrm{s1}}$ and twist angle θ, they are not fixed in the Brillouin zone (BZ), i.e., they are removable. Note that their positions are independent of the strength of d-wave pairing Δ_{d}. If the number of FSs enclosing a DPN is odd, there will be at least one FS that cannot shrink to disappear without bypassing the DPN (other FSs can be canceled in pairs). This implies that the energy band cannot adiabatically evolve to a vacuum, and therefore the system is in the topologically non-trivial phase.

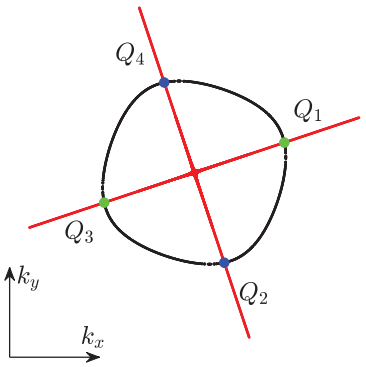


Fig. 2. The nodal lines of d-wave (red line) and $s_\pm$-wave (black line) superconductors. Four Dirac pairing nodes are denoted by $\boldsymbol{Q}_i$ $(i=1,2,3,4)$.

However, those four DPNs are connected through a C_4 operation due to that the nodal lines of $\Delta_a(\boldsymbol{k}_a)$ and $\Delta_b(\boldsymbol{k}_b)$ [see Appendix Eqs. (A5) and (A6)] have quadruple rotational symmetry (i.e., C_4 symmetry). Consequently, if the FS of the normal state is also C_4 invariant, these four DPNs will be enclosed by a FS at the same time. This may lead to either topologically trivial or second-order topological phases.[21,29] In order to achieve first-order topological phases, it is necessary to break the C_4 symmetry of the FS. In this paper, we propose two approaches to realize this: Rashba and Dresselhaus mixed SOC and anisotropic nearest neighbor hopping with $t_x\neq t_y$.[21,30] As long as one of them is present in the system, it is possible to achieve any form of encirclement of FS into a removable DPN and induce a topological phase transition by adjusting the chemical potential (which controls the size of FS) or the twist angle (which controls the orientation of FS).

At a commensurate twisted angle of $\theta=53.13^\circ$, the Moiré lattice forms. Topological quantities such as the Chern number can be computed exactly using the Moiré momentum $\tilde{\boldsymbol{k}}$,[27,31] no matter what type of interlayer hopping is. The area of Moiré BZ is one-fifth of that of BZ of the original square lattice. As illustrated in Fig. 3, topological phases with Chern number $C=\pm2$ exist in the phase diagram in the $(\mu,\Delta_{\mathrm{s0}}/\Delta_{\mathrm{s1}})$ plane, for both the mixed SOC system in panel (a) and the anisotropic nearest neighbor hopping system in panel (b). The mixed SOC term and the anisotropic nearest neighbor hopping break the C_4 symmetry of the FSs (see Fig. 4), giving rise to richer relative configurations between FSs and DPNs. To demonstrate the effect of the twisted angle, we also present in Fig. 3(c) the phase diagram of the mixed SOC system at twisted angle $\theta=0^\circ$. The topologically non-trivial regions in Fig. 3(c) are larger than those in Fig. 3(a), and especially a topological phase with $C=-4$ appears. However, there is no first-order topological phase in the phase diagram (not shown) of the anisotropic nearest neighbor hopping system at $\theta=0^\circ$. By turning on the twisted angle, the orientation of FS will change and eventually modify the encirclement of DPNs.

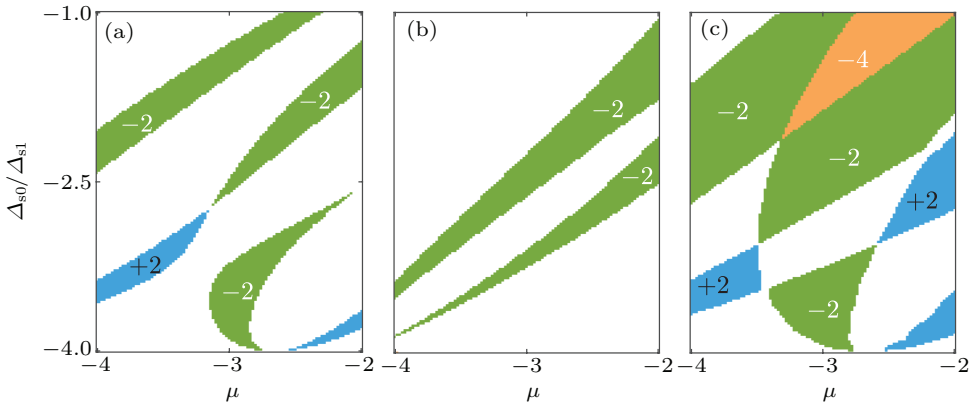


Fig. 3. The topological phase diagram at a twisted angle of $\theta = 53.13°$ for a mixed SOC system (a) and an anisotropic nearest neighbor hopping system (b). The colored area represents topological non-trivial phases. For panel (a), the parameters are $t_x = t_y = 1, \lambda_R = 0.25, \lambda_D = -0.5$; for panel (b), the parameters are $t_x = 1, t_y = 0.5, \lambda_R = 0.25, \lambda_D = 0$. The interlayer tunneling magnitude is $g_0 = 0.25$. Panel (c) is similar to panel (a) except that the twist angle is $\theta = 0°$.

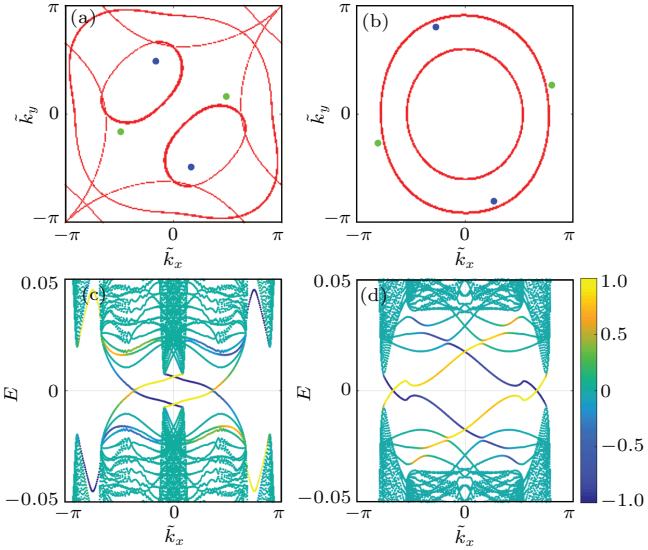


Fig. 4. The Fermi surface and Dirac pairing nodes at a twisted angle of $\theta = 53.13°$ for the mixed SOC system (a) and the anisotropic nearest neighbor hopping system (b). The green (blue) dot denotes the pairing node. Panel (a) corresponds to a point in the phase diagram of Fig. 3(a) with $(\mu, \Delta_{s0}/\Delta_{s1}) = (-2.9, -3.5)$. Panel (b) corresponds to a point in the phase diagram of Fig. 3(b) with $(\mu, \Delta_{s0}/\Delta_{s1}) = (-3.3, -2.74)$. The superconducting parameters are chosen as $\Delta_d = 0.05$ and $\Delta_{s0} = 0.3$. Other values of parameters used in panels (a) and (b) are identical to those in Figs. 3(a) and 3(b), respectively. Panel (c) and (d) show the energy spectrum on an infinite cylinder geometry, corresponding to panels (a) and (b), respectively. The color scale shows the expectation value $\hat{y}$ of the eigenstates, where $\hat{y}$ denotes the position along the open direction of cylinder and its range is normalized to $[-1, 1]$. Along the open direction, 180 Moiré unit cells are used in the calculations.

To further illustrate the topological phase, we choose two typical points in the phase diagram of Figs. 3(a) and 3(b), and plot their FSs in Figs. 4(a) and 4(b), respectively. Due to the breaking of C_4 rotation symmetry, the FSs are distorted and enclose only two blue nodes in both Figs. 4(a) and 4(b), resulting in a non-zero Chern number of -2. Moreover, we plot the energy spectrum on an infinite cylinder geometry in Figs. 4(c) and 4(d). From these figures, one can observe a fully gapped bulk spectrum and two chiral edge modes, which exactly match with the Chern number. Note that the position of pairing nodes and the topological phase diagram are determined only by the ratio Δ_{s0}/Δ_{s1}, but the bulk band gaps in Figs. 4(c) and 4(d) do depend on the gap magnitude Δ_d and Δ_{s0} (or Δ_{s1}).

4. Conclusion

In summary, we study the topological properties of twisted bilayer superconductors composed of $s_\pm$-wave and d-wave pairings. By performing the chirality basis transformation to the bilayer system, we reveal that the topological phase depends on the non-trivial enclosing relation between FSs and DPNs. It is found that the C_4 rotation symmetry-breaking terms, i.e., mixed Rashba and Dresselhaus SOC and anisotropic nearest-neighbor hopping, are essential to realize the first-order topological phase. The effect of the twisted angle on these two C_4 breaking systems is quite different: It creates a phase with $C = -2$ in the anisotropic hopping system, but annihilates the $C = -4$ phase in the mixed SOC system. Finally, we calculate the edge spectrum using Moiré lattice at a twisted angle of 53.13°. The obtained chiral edge modes are in good agreement with the Chern number, as well as the enclosing relation between FSs and DPNs.

Appendix A

The BdG Hamiltonian $H_{\mathrm{BdG},\theta}(\boldsymbol{k})$ in Eq. (10) of the main text can be written as

$$H_{\mathrm{BdG},\theta}(\boldsymbol{k}) = \begin{pmatrix} H_a(\boldsymbol{k}_a) & T \\ T & H_b(\boldsymbol{k}_b) \end{pmatrix}, \tag{A1}$$

in which $T = t_z(\boldsymbol{k}_a, \boldsymbol{k}_b)\sigma_0\tau_z$ is a 4×4 matrix for interlayer tunneling,[32,33] the $\boldsymbol{\sigma}$ and τ here are the Pauli matrices in spin and particle–hole spaces. $H_l(\boldsymbol{k}_l)$ is the Hamiltonian of l layer,

$$H_l(\boldsymbol{k}_l) = \begin{pmatrix} \xi_l(\boldsymbol{k}_l)\sigma_0 + \boldsymbol{L}_l(\boldsymbol{k}_l)\cdot\boldsymbol{\sigma} & \mathrm{i}\Delta_l(\boldsymbol{k}_l)\sigma_y \\ -\mathrm{i}\Delta_l^*(\boldsymbol{k}_l)\sigma_y & -\xi_l(\boldsymbol{k}_l)\sigma_0 + \boldsymbol{L}_l(\boldsymbol{k}_l)\cdot\boldsymbol{\sigma}^{\mathrm{T}} \end{pmatrix}. \tag{A2}$$

The electron dispersion in each layer reads

$$\xi_l(\boldsymbol{k}_l) = -2t_x \cos k_{l,x} - 2t_y \cos k_{l,y} - \mu, \tag{A3}$$

the vector of SOC $\boldsymbol{L}_l(\boldsymbol{k}_l) = (\lambda_{xl}, \lambda_{yl}, \lambda_{zl})$ is given by

$$\begin{aligned}&(\lambda_{xl}, \lambda_{yl}, \lambda_{zl})\\ &= -2\left(\lambda_{\mathrm{R}} \sin k_{l,y} + \lambda_{\mathrm{D}} \sin k_{l,x}, -\lambda_{\mathrm{R}} \sin k_{l,x} - \lambda_{\mathrm{D}} \sin k_{l,y}, 0\right),\end{aligned} \tag{A4}$$

the superconducting gap functions $\Delta_l(\boldsymbol{k}_l)$ are

$$\Delta_a(\boldsymbol{k}_a) = 2\Delta_{\mathrm{d}}\left(\cos k_{a,x} - \cos k_{a,y}\right), \tag{A5}$$

$$\Delta_b(\boldsymbol{k}_b) = \mathrm{i}\Delta_{\mathrm{s}0} + 2\mathrm{i}\Delta_{\mathrm{s}1}\left(\cos k_{b,x} + \cos k_{b,y}\right). \tag{A6}$$

We introduce the following similar transformation G to project the Hamiltonian into chirality basis representation:[13]

$$G = \begin{pmatrix} g_a & 0 \\ 0 & g_b \end{pmatrix}, \quad g_l = \frac{1}{\sqrt{2\zeta_l^2}} \begin{pmatrix} U_l^{\dagger}(\boldsymbol{k}_l) & 0 \\ 0 & U_l^{\mathrm{T}}(-\boldsymbol{k}_l) \end{pmatrix}, \tag{A7}$$

$$U_l(\boldsymbol{k}_l) = \begin{pmatrix} \lambda_{xl} - \mathrm{i}\lambda_{yl} & -\zeta_l \\ \zeta_l & \lambda_{xl} + \mathrm{i}\lambda_{yl} \end{pmatrix}, \tag{A8}$$

with $\zeta_l = \sqrt{\lambda_{xl}^2 + \lambda_{yl}^2}$. The Hamiltonian has a new form

$$\tilde{H}_{\mathrm{BdG},\theta}(\boldsymbol{k}) = G H_{\mathrm{BdG},\theta}(\boldsymbol{k}) G^{\dagger} = \begin{pmatrix} \tilde{H}_a(\boldsymbol{k}_a) & \tilde{T} \\ \tilde{T}^{\dagger} & \tilde{H}_b(\boldsymbol{k}_b) \end{pmatrix}, \tag{A9}$$

in which the matrices $\tilde{H}_l(\boldsymbol{k}_l)$ and $\tilde{T}$ are given by

$$\tilde{H}_l(\boldsymbol{k}_l) = \begin{pmatrix} \xi_l(\boldsymbol{k}_l) + \zeta_l \sigma z & \tilde{\Delta}_l(\boldsymbol{k}_l) \\ \tilde{\Delta}_l^{\dagger}(\boldsymbol{k}_l) & -\xi_l(\boldsymbol{k}_l) - \zeta_l \sigma_z \end{pmatrix}, \tag{A10}$$

$$\tilde{\Delta}_l(\boldsymbol{k}) = \frac{1}{2\zeta_l} \begin{pmatrix} \Delta_l(\boldsymbol{k}_l)(\lambda_{xl} - \mathrm{i}\lambda_{yl}) & 0 \\ 0 & \Delta_l(\boldsymbol{k}_l)(\lambda_{xl} + \mathrm{i}\lambda_{yl}) \end{pmatrix}, \tag{A11}$$

$$\begin{aligned}\tilde{T} &= g_a T g_b^{\dagger}\\ &= \frac{t_z(\boldsymbol{k}_a, \boldsymbol{k}_b)}{2\zeta_a\zeta_b} \begin{pmatrix} U_a^{\dagger}(\boldsymbol{k}_a) U_b(\boldsymbol{k}_b) & 0 \\ 0 & -U_a^{\mathrm{T}}(-\boldsymbol{k}_a) U_b^{*}(-\boldsymbol{k}_b) \end{pmatrix}.\end{aligned} \tag{A12}$$

To gain a deeper understanding of Hamiltonian $\tilde{H}_{\mathrm{BdG},\theta}(\boldsymbol{k})$, we exchange the 3rd and 4th rows (and columns) with the 5th and 6th rows (and columns), respectively. This will transfer the matrix elements that involve superconducting pairing to the block matrix on the off-diagonal. Finally, the Hamiltonian can be rewritten as

$$H_{\mathrm{odd},\theta}(\boldsymbol{k}) = \begin{pmatrix} \Sigma_{\theta}(\boldsymbol{k}) & \Delta_{\mathrm{odd},\theta}(\boldsymbol{k}) \\ \Delta_{\mathrm{odd},\theta}^{\dagger}(\boldsymbol{k}) & -\boldsymbol{\Sigma}_{\theta}^{\mathrm{T}}(-\boldsymbol{k}) \end{pmatrix}, \tag{A13}$$

$$\Sigma_{\theta}(k) = \begin{pmatrix} \xi_a(\boldsymbol{k}_a) + \zeta_a \sigma_z & \dfrac{t_z(\boldsymbol{k}_a, \boldsymbol{k}_b) U_a^{\dagger}(\boldsymbol{k}_a) U_b(\boldsymbol{k}_b)}{2\zeta_a\zeta_b} \\ \dfrac{t_z(\boldsymbol{k}_a, \boldsymbol{k}_b) U_b^{\dagger}(\boldsymbol{k}_b) U_a(\boldsymbol{k}_a)}{2\zeta_a\zeta_b} & \xi_b(\boldsymbol{k}_b) + \zeta_b \sigma_z \end{pmatrix}, \tag{A14}$$

$$\Delta_{\mathrm{odd},\theta}(\boldsymbol{k}) = \begin{pmatrix} \tilde{\Delta}_a(\boldsymbol{k}_a) & 0 \\ 0 & \tilde{\Delta}_b(\boldsymbol{k}_b) \end{pmatrix}. \tag{A15}$$

Acknowledgements

Stimulating discussions with Zhenghao Yang are gratefully acknowledged.

Project supported by the National Natural Science Foundation of China (Grant No. 11974293).

References

[1] Sato M and Ando Y 2017 *Rep. Prog. Phys.* **80** 076501
[2] Stern A and Lindner N H 2013 *Science* **339** 1179
[3] Pfaff W, Hensen B J, Bernien H, Van Dam S B, Blok M S, Taminiau T H, Tiggelman M J, Schouten R N, Markham M, Twitchen D J and Hanson R 2014 *Science* **345** 532
[4] Freedman M H, Kitaev A Y, Larsen M and Wang Z 2001 *Bulletin of the American Mathematical Society* **40** 31
[5] Tewari S, Das Sarma S, Nayak C, Zhang Chuanwei and Zoller P 2007 *Phys. Rev. Lett.* **98** 010506
[6] Ivanov D A 2001 *Phys. Rev. Lett.* **86** 268
[7] Can O, Tummuru T, Day R P, Elfimov I, Damascelli A and Franz M 2021 *Nat. Phys.* **17** 519
[8] Yang Z, Qin S, Zhang Q, Fang C and Hu J 2018 *Phys. Rev. B* **98** 104515
[9] Tummuru T R, Lantagne-Hurtubise E and Franz M 2022 *Phys. Rev. B* **106** 014520
[10] Song X Y, Zhang Y H and Vishwanath A 2022 *Phys. Rev. B* **105** L201102
[11] Mercado A, Sahoo S and Franz M 2022 *Phys. Rev. Lett.* **128** 137002
[12] Margalit G, Yan B, Franz M and Oreg Y 2022 *Phys. Rev. B* **106** 205424
[13] Sato M, Takahashi Y and Fujimoto S 2010 *Phys. Rev. B* **82** 134521
[14] Sato M, Takahashi Y and Fujimoto S 2009 *Phys. Rev. Lett.* **103** 020401
[15] Laughlin R B 1998 *Phys. Rev. Lett.* **80** 5188
[16] Yu Y, Ma L, Cai P, Zhong R, Ye C, Shen J, Gu G D, Chen X H and Zhang Y 2019 *Nature* **575** 156
[17] Lee W C, Zhang S C and Wu C 2009 *Phys. Rev. Lett.* **102** 217002
[18] Ishida K, Nakai Y and Hosono H 2010 *J. Phys. Soc. Jpn.* **78** 062001
[19] Mazin I I 2010 *Nature.* **464** 183
[20] Zhu X 2019 *Phys. Rev. Lett.* **122** 236401
[21] Kheirkhah M, Yan Z, Nagai Y and Marsiglio F 2020 *Phys. Rev. Lett.* **125** 017001
[22] Gotlieb K, Lin C Y, Serbyn M, Zhang W, Smallwood C L, Jozwiak C, Eisaki H, Hussain Z, Vishwanath A and Lanzara A 2018 *Science* **362** 1271
[23] Park M J, Kim Y, Cho G Y and Lee S 2019 *Phys. Rev. Lett.* **123** 216803
[24] Kindermann M 2015 *Phys. Rev. Lett.* **114** 226802
[25] Bistritzer R and MacDonald A H 2011 *Proc. Natl. Acad. Sci. USA* **108** 12233
[26] Hejazi K, Liu C, Shapourian H, Chen X and Balents L 2019 *Phys. Rev. B* **99** 035111
[27] Fukui T, Hatsugai Y and Suzuki H 2005 *J. Phys. Soc. Jpn.* **74** 1674
[28] Sato M 2010 *Phys. Rev. B* **81** 220504
[29] Yan Z 2019 *Phys. Rev. Lett.* **123** 177001
[30] Hai K, Zhu W, Chen Q and Hai W 2020 *Chin. Phys. B* **29** 083203
[31] Dong B, Yang T and Han Z 2020 *Chin. Phys. B* **29** 097307
[32] Volkov P A, Zhao F S Y, Poccia N, Cui X, Kim P and Pixley J H 2021 arXiv: 2108.13456 [cond-mat.supr-con]
[33] Volkov P A, Wilson J H, Lucht K P and Pixley J H 2023 *Phys. Rev. Lett.* **130** 186001